

Robust and Repeatable Biofabrication of Bacteria-Mediated Drug Delivery Systems: Effect of Conjugation Chemistry, Assembly Process Parameters, and Nanoparticle Size

Ying Zhan¹, Austin Fergusson¹, Lacey R. McNally¹, Richey M. Davis¹, and Bahareh Behkam¹

¹Affiliation not available

October 25, 2021

Abstract

Bacteria-mediated drug delivery systems comprising nanotherapeutics conjugated onto bacteria synergistically augment the efficacy of both therapeutic modalities in cancer therapy. Nanocarriers preserve therapeutics' bioavailability and reduce systemic toxicity, while bacteria selectively colonize the cancerous tissue, impart intrinsic and immune-mediated antitumor effects, and propel nanotherapeutics interstitially. The optimal bacteria-nanoparticle (NP) conjugates would carry the maximal NP load with minimal motility speed hindrance for effective interstitial distribution. Furthermore, a well-defined and repeatable NP attachment density distribution is crucial to determining these biohybrid systems' efficacious dosage and robust performance. Herein, we utilized our Nanoscale Bacteria-Enabled Autonomous Delivery System (NanoBEADS) platform to investigate the effects of assembly process parameters of mixing method, volume, and duration on NP attachment density and repeatability. We also evaluated the effect of linkage chemistry and NP size on NP attachment density, viability, growth rate, and motility of NanoBEADS. We show that the linkage chemistry impacts NP attachment density while the self-assembly process parameters affect the repeatability and, to a lesser extent, attachment density. Lastly, the attachment density affects NanoBEADS' growth rate and motility in an NP size-dependent manner. These findings will contribute to the development of scalable and repeatable bacteria-nanoparticle biohybrids for applications in drug delivery and beyond.

Corresponding author(s) Email: behkam@vt.edu

ToC Figure

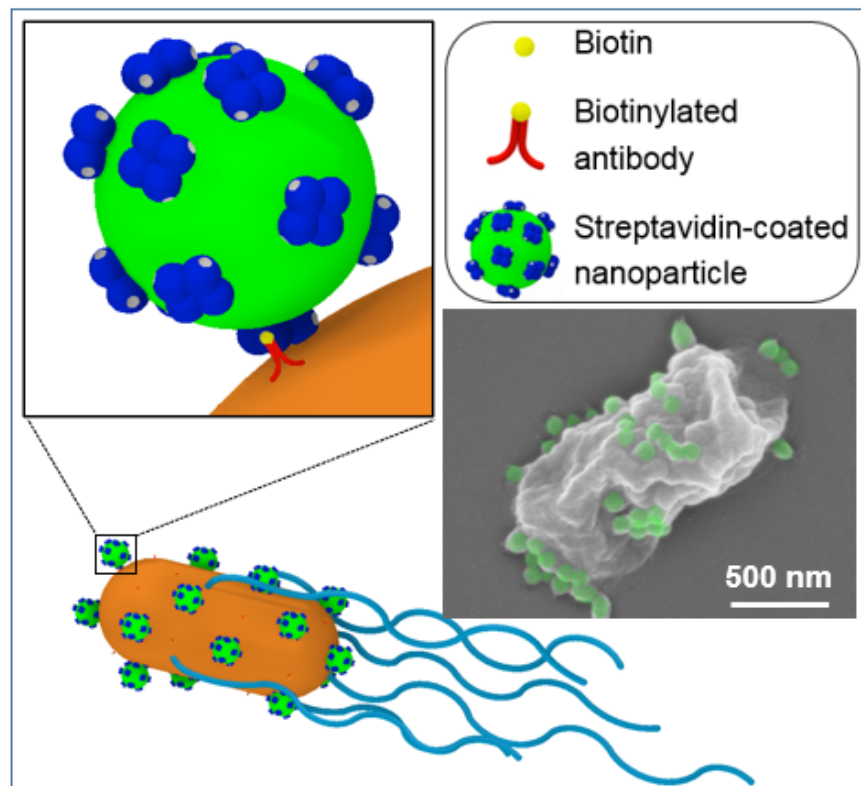


Figure 1: **ToC Figure.** Bacteria-nanoparticle biohybrids enhance interstitial transport of nanomedicine via self-propulsion. Herein, we show the significant effect of linkage chemistry and assembly process parameters of mixing method, duration, and volume on the density and repeatability of nanoparticle attachment. We further report the effect of nanoparticle size and attachment density on the growth rate and motility of bacteria-nanoparticle conjugates.

Introduction

Biohybrid or cell-mediated drug delivery systems, also referred to as biohybrid microrobots, consist of nanocarriers conjugated with host cells,(Stephan et al., 2010)(Mooney et al., 2014)(Huang et al., 2015)(Villa et al., 2016)(Choi et al., 2007)(Roger et al., 2010) attenuated pathogens,(Akin et al., 2007)(Traore et al., 2014)(Suh et al., 2018b) or generally regarded as safe (GRAS) microorganisms,(Xie et al., 2017) which are harnessed as *living machines* for transport of therapeutic loads (for a recent comprehensive review, see ref(Bastos-Arrieta et al., 2018)(Schmidt et al., 2020)). In contrast to the traditional systemically administered therapeutics, bio-hybrid microrobotic systems for drug delivery are capable of active and targeted delivery using a variety of motility mechanisms (i.e., actuation for self-propulsion) and receptors (i.e., sensors) that enable the cells to process and respond to external signals from their environment, including other cells. The innate actuation and sensing mechanisms powered by chemical energy harvested from the environment provide a distinct advantage to biohybrid microrobots, compared to fully synthetic microrobotic systems that typically rely on external electrical, magnetic, optical, or acoustic sources of energy for controlled actuation. Thus, biohybrid microrobots have considerable potential for targeted delivery of drugs, genes, mRNA, proteins, imaging contrast agents, and radioactive seeds to specific target locations accessible vascularly, orally, or even interstitially. In particular, bacteria possess unique properties of high speed (up to ~ 50 body lengths per second) self-propulsion through blood,(Gekle, 2016) mucus,(Celli et al., 2009) and tissue,(Toley and Forbes, 2012) biased migration or taxis in response to a variety of stimuli (e.g., chemotaxis,(Adler, 1966)

aerotaxis,(Taylor et al., 1999) magnetotaxis,(Faivre and Schüler, 2008) phototaxis,(Bhaya, 2004)(Taylor and Koshland, 1975) and pH-taxis(Kihara and Macnab, 1981)), and can be genetically manipulated to produce attenuated or auxotrophic strains,(Clairmont et al., 2000)(Low et al., 1999)(Zhao et al., 2005) which support safe and selective colonization of bacteria *in vivo*.(Toso, 2002)(Heimann and Rosenberg, 2003)(Nemunaitis et al., 2003)(Le et al., 2012)(Roberts et al., 2014)(Schmitz-Winnenthal et al., 2018)(Le et al., 2015)(Basu et al., 2018) Altogether, the advantages of targeted accumulation, deep penetration through self-propulsion, and straightforward genetic manipulation, make bacteria an ideal candidate for targeted therapeutic delivery.

Bacteria-based bio-hybrid drug delivery systems are comprised of live bacteria, for sensing and controlled transport, and abiotic micro- or nano-particles as cargo. Construction of an effective bio-hybrid drug delivery system requires an attachment mechanism that is stable *in vivo* and is amenable to interstitial transport, yields sufficient and repeatable cargo attachment density for a predictable therapeutic outcome, and does not render the bacteria non-motile. Electrostatic interactions, (Behkam and Sitti, 2008)(van Loosdrecht et al., 1990) hydrophobic interactions,(van Loosdrecht et al., 1990) covalent binding,(Xie et al., 2017)(Felfoul et al., 2016)(Taherkhani et al., 2014) bioaffinity interactions,(Traore et al., 2014)(Kazmierczak et al., 2014)(Nguyen et al., 2016)(Alapan et al., 2018) antibody-antigen interactions,(Xu et al., 2012) or a combination thereof,(Akin et al., 2007)(Traore et al., 2014)(Alapan et al., 2018)(Kojima et al., 2012) have been used to attach nanoparticles (NP) to bacteria. Although various attachment methodologies have been explored, a systematic investigation of the effect of the conjugation chemistry and the assembly process parameters on the NP attachment density and repeatability has not been attempted before. Furthermore, the effect of NP load size and quantity on bacterial motility and growth is rarely explored. In this work, we used our previously developed bacteria-based bio-hybrid platform, known as Nanoscale Bacteria-Enabled Autonomous Drug Delivery System (NanoBEADS),(Traore et al., 2014) to investigate the aforementioned questions. Two linkage chemistries were separately utilized to attach poly(lactic-co-glycolic acid) (PLGA) NPs to the tumor-targeting *S. Typhimurium* VNP20009 *cheY*⁺ bacteria, as shown in **Figure 2**. The effect of assembly process parameters of mixing method, volume, and duration on the NP attachment density and repeatability was investigated. Subsequently, for the two best performing sets of assembly parameters, the effect of linkage chemistry and NP size on NP attachment density, viability, growth rate, and motility of NanoBEADS was studied. We found the linkage chemistry most significantly affected the NP attachment density. For each of the two binding mechanisms tested, the assembly process parameters also influenced NP attachment's areal density and repeatability. Furthermore, the increase in the NP load-carrying capacity led to an increase in doubling time and a reduction in NanoBEADS motility speed in an NP size-dependent manner.

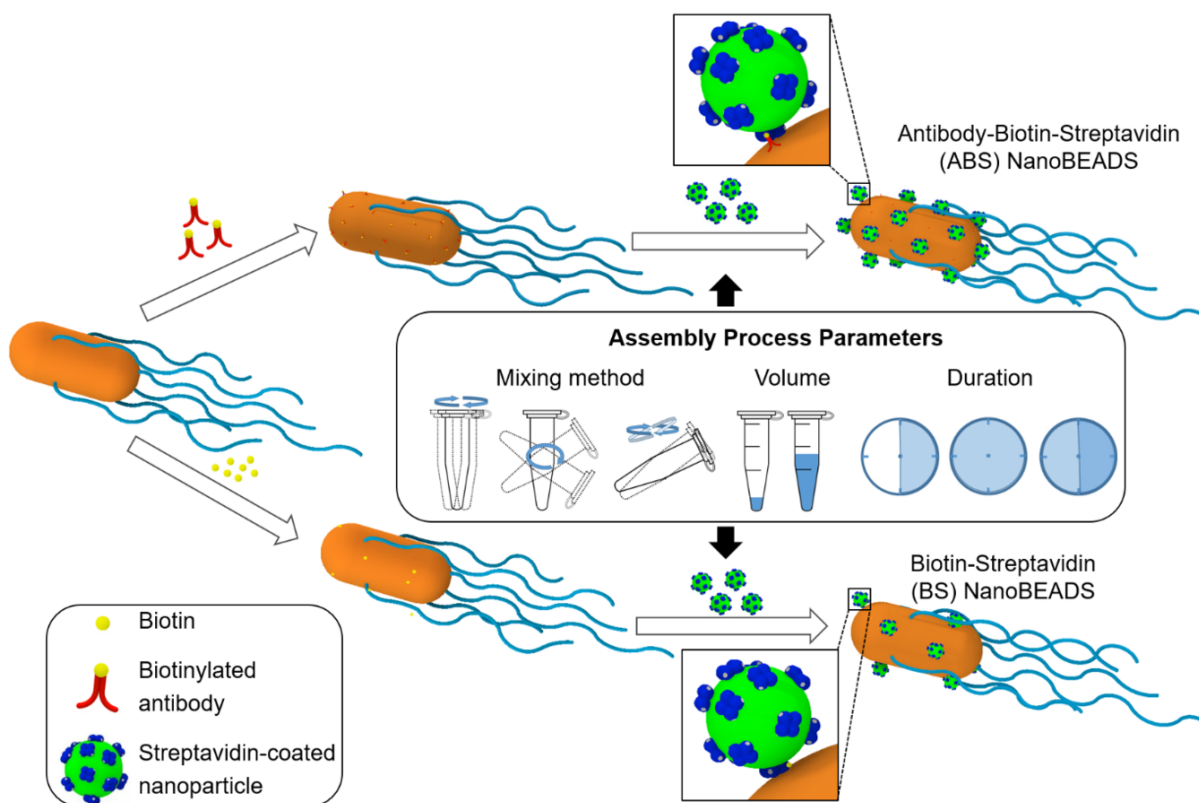


Figure 2: Construction of the Nanoscale Bacteria-Enabled Drug Delivery System (NanoBEADS). Schematic of the self-assembly process of two NanoBEADS variants- Antibody-Biotin-Streptavidin NanoBEADS (ABS NanoBEADS) and Biotin-Streptavidin NanoBEADS (BS NanoBEADS). The conjugation chemistry and assembly process parameters of mixing method, volume, and duration affect the density and repeatability of the nanoparticle attachment outcomes.

Experimental Section/Methods

Bacteria preparation: *Salmonella* Typhimurium VNP20009 *cheY*⁺ (Broadway et al., 2017) from a single colony was cultured overnight in MSB medium (10 g/L tryptone, and 5 g/L yeast extract, 2 mM MgSO₄, 2mM CaCl₂, pH 7.0) at 37°C and 100 rpm (Excella E24 Incubator Shaker Series, New Brunswick Scientific). The overnight bacterial culture was diluted in MSB to 1% (v/v) and incubated at 37°C and 100 rpm until an optical density at 600 nm (OD₆₀₀) of 1.0 was reached. The bacterial culture was centrifuged at 1,700 ×g for 5 minutes twice and re-suspended in motility buffer (6.4 mM K₂HPO₄, 3.5 mM KH₂PO₄, 1 μM L-methionine, 10 mM Sodium DL-lactate, 2 mM MgSO₄, 2 mM CaCl₂, pH 7.0) to a final OD₆₀₀ of 1.0.

PLGA Nanoparticle Synthesis: 100 mg of Pluronic[®] F127 and 20 mL of deionized water were added to a glass vial. The vial was placed in a water bath sonicator (Branson 2510 Ultrasonic Cleaner, 100 W) for 30 minutes to dissolve the Pluronic. Then, a magnetic stir bar was added, and the solution was stirred at 600 rpm. Acid-terminated PLGA (Mw: 25,000 g mol⁻¹, 50:50 lactic acid:glycolic acid, acid end-capped, Akina Inc. PolySciTech, West Lafayette, IN) was dissolved with dimethylformamide (DMF, Sigma-Aldrich, St. Louis, MO) to a final concentration of 22.22 mg/mL; the solution was sonicated for 30 minutes to ensure molecular dissolution. While the PLGA solution was sonicating, 6,13-bis(triisopropylsilylethynyl) pentacene (TIPS, Sigma-Aldrich, St. Louis, MO) was dissolved in tetrahydrofuran (THF, anhydrous and uninhibited,

>99.9%, Sigma-Aldrich, St. Louis, MO) to a final concentration of 3.05 mg/mL. After the PLGA solution was fully dissolved, TIPS solution was added to the PLGA solution to achieve a 1:10 THF:DMF volume ratio. The mixture was vortexed for ~5 seconds before it was loaded into a 5 mL glass syringe with a 21-gauge needle attached. Care was taken to remove all macroscopic air bubbles from the syringe. The TIPS:PLGA mixture (1 mL) was added dropwise (0.5 mL/min, NE-1000, New Era Pump Systems Inc.) to the stirring (600 rpm) Pluronic F127 solution. The resulting nanoparticle suspension was allowed to stir for 5 hours at 600 rpm. The suspension was protected from light to prevent degradation of the fluorophore. After 5 hours, the suspension was centrifuged at 22,789 $\times g$ for 30 minutes at 4°C (Sorvall Legend X1R, ThermoFisher Scientific). The supernatant was discarded. The pellet was resuspended in 20 mL of 1x PBS by vortex mixing for 2 minutes and sonicating the suspension for 30 minutes. The final dispersed suspension was passed through a nitrocellulose syringe filter (0.45 μm pore size) to remove any remaining aggregates. The filtrate was stored in a foil-wrapped vial at room temperature.

Streptavidin Functionalization of PLGA Nanoparticles: Microcentrifuge tubes were filled with 700 μL of PLGA NP suspension. The tubes were centrifuged at 16,060 $\times g$ for 10 minutes at room temperature (accuSpin Micro, Fisher Scientific). The pellets were resuspended in 800 μL of EDAC coupling solution (20 mg/mL EDAC, 5 $\mu g/mL$ streptavidin-Cy3, pH 5.2 50 mM MES buffer). The streptavidin coupling reaction took place on a vortex mixer (500 rpm, Fisher Digital Vortex 120V, Fisher Scientific) for 3 hours. Following streptavidin coupling, the microcentrifuge tubes were centrifuged at 16,060 $\times g$ for 10 minutes at room temperature. The pellets were resuspended in 100 μL of motility buffer.

Dynamic Light Scattering (DLS) Measurements: DLS measurements were performed using a Zetasizer Nano ZS (Malvern Instruments) operating with Zetasizer Software v7.12. Disposable polystyrene cuvettes were filled with 1 mL of the final aqueous nanoparticle suspensions. Measurements were performed at room temperature, and the results are shown in **Figure S6** and **Table S1**.

Zeta Potential Measurements: The final aqueous nanoparticle suspensions were loaded into disposable polystyrene capillary cells. Zeta potential measurements were performed using a Zetasizer Nano ZS at room temperature. The results are shown in Figure S6 and Table S1.

Nanoparticle Tracking Analysis (NTA): Dilutions (10 \times and 100 \times) of the functionalized nanoparticle suspensions were analyzed via nanoparticle tracking analysis using a NanoSight NS500 (Malvern Instruments) operating with NanoSight NTA v3.4. All measurements were performed at room temperature. Five 1-minute videos were taken for each sample, and the nanoparticle scattering cones were tracked to determine the number concentrations of the nanoparticle suspensions before incubating the nanoparticles with bacteria to form NanoBEADS.

PLGA NanoBEADS assembly: To prepare the ABS NanoBEADS, the prepared bacterial suspension in motility buffer was incubated with 10 $\mu g/mL$ biotinylated *Salmonella* polyclonal antibody (Thermo Scientific, Waltham, MA, USA) on a vortex mixer at 500 rpm at room temperature for 1 hr. The antibody-coated bacteria suspension was then centrifuged at 1,700 $\times g$ for 5 minutes to remove free antibody and suspended in motility buffer to an OD₆₀₀ of 2.0 (Cary 60 UV-Vis, Agilent Technologies). Next, the suspension of biotinylated antibody-coated bacteria was mixed with the streptavidin-coated nanoparticle at a bacteria to particles ratio of 1:100 in a volume of 100 μL or 800 μL (as described in Table 1) and incubated on a vortex mixer at 500 rpm, a Belly Dancer[®] mixer (IBI Scientific) at 100 rpm, or an end-over-end mixer (Fisher Scientific) at 15 rpm for 30 minutes, 60 minutes or 90 minutes to facilitate the assembly of nanoparticles onto the bacteria. For BS NanoBEADS, the bacterial suspension in the motility buffer was incubated with 0.4 mg/mL biotin (Fisher BioReagents, Fair Lawn, NJ) on a vortex mixer at 500 rpm at room temperature for 30 minutes to physisorb biotin onto bacteria. Subsequently, the suspension was centrifuged at 1,700 $\times g$ for 5 minutes to remove free biotin and resuspended the biotin-coated bacteria in motility buffer to an OD₆₀₀ of 2.0. Next, the suspension of bacteria coated with biotin was mixed with the streptavidin-coated nanoparticles at a bacteria to particles ratio of 1:100 in a volume of 800 μL and incubated on a belly dancer mixer at 100 rpm or an end over end mixer at 15 rpm for 60 minutes. After the assembly process, the suspension of NanoBEADS was transferred to a centrifugal filter unit with a 0.8 μm pore size high-flux polyethersulphone

membrane (Sartorius Vivaclear, Elk Grove, IL) and centrifuged at $1,700 \times g$ for 30 seconds to remove free nanoparticles. The NanoBEADS were suspended in motility buffer to an OD_{600} of 1.0 for NP areal density characterization experiments or in McCoy's 5A for the growth and motility assays.

NanoBEADS samples preparation for field emission scanning electron microscope (FE-SEM): To quantify the number of nanoparticles attached to the outer membrane of bacteria, SEM images of NanoBEADS were taken using FE-SEM. A 10 μ L aliquot of the NanoBEADS suspension was deposited on 0.005% (w/v) poly-L-lysine (PLL) treated glass slides and incubated at room temperature for 5 minutes to allow for attachment. Afterward, the slide was rinsed in DI water to remove the loosely attached nanoparticles and NanoBEADS. Then, the slide was covered with 4% glutaraldehyde for 2 hours at 4°C to fix the attached NanoBEADS. Next, the slide was soaked in 0.1 M Phosphate-buffered saline (PBS) for 20 minutes twice. Finally, the same soaking process was repeated with deionized water. After air-drying overnight, the slide was sputter-coated with 7 nm Pt/Pd prior to imaging (Leica ACE600 sputter). High-resolution images were obtained utilizing a LEO (Zeiss) 1550 FE-SEM at an accelerating voltage of 5 kV and working distances of <8.6 mm. To determine the average number of attached nanoparticles for each NanoBEADS experiment, the particle numbers on ~ 50 bacteria were counted for each replicate. A minimum of two independent experiments were carried out for each case.

Viability assay: The filtered NanoBEADS were diluted in motility buffer to an OD_{600} of 0.05. To this 1 mL diluted NanoBEADS solution, 1.5 μ L aliquots of the 3.34 mM SYTO 9 nucleic acid stain and 20 mM propidium iodide (LIVE/DEAD[®] BacLight Bacterial Viability Kit, Thermo Fisher, Eugene, Oregon, USA) were added, followed by incubation in the dark at room temperature for 15 minutes as per the manufacturer's instructions. The fluorescence microscopy images of NanoBEADS were taken using a Zeiss AxioObserver Z1 inverted microscope equipped with an AxioCam mRM camera at 40x objective. Live cells with an intact membrane stained green only, where cells with a damaged membrane or dead cells also stained red.

Growth rate measurement: The NanoBEADS suspensions were diluted in 3 mL of McCoy's 5A medium supplemented with 10% FBS to a final OD_{600} of 0.001. The diluted NanoBEADS suspension was incubated at 37degC with shaking at 100 rpm for 10 hours. A 100 μ L sample was taken every hour, diluted, and plated on triplicate 1.5% LB agar plates. Following overnight incubation at 37°C, the bacteria colonies on the agar plates were counted to determine the NanoBEADS growth rate. A minimum of two independent experiments were carried out for each case.

Swimming speed measurement: The bacterial and NanoBEADS suspensions were diluted in 3 mL of McCoy's 5A medium supplemented with 10% FBS to a final OD_{600} of 0.001. The diluted suspensions were incubated at 37°C with shaking at 100 rpm for 2 hours. A 10 μ L sample was taken, diluted, and placed on the glass coverslip. The videos of the bacteria movement were taken with a Zeiss AxioObserver Z1 inverted microscope equipped with an AxioCam Hsm camera and 63 \times oil immersion objective. The videos were analyzed in ImageJ using the MTrackJ plug-in tool. The average swimming speed was calculated by averaging the instantaneous speed, which is the traveled distance in each unit of time divided by the time unit. For each experiment, about 50 bacteria or NanoBEADS were tracked in the 15 s videos acquired at 32.8 fps. A minimum of two independent experiments were carried out for each case.

Results and Discussion

The Effect of the assembly process parameters on NP attachment density

The NP attachment density is critical to the efficacy of bacteria-based drug delivery systems, as it determines the amount of therapeutic load carried by each NanoBEADS agent. We first investigated the effect of mixing method (i.e., the type of mechanical mixer employed when mixing the streptavidin-coated NPs and

the biotinylated bacterial suspensions, **Video S1**), assembly volume (i.e., total suspension volume during mixing), and assembly period, as depicted in **Table 1**, on the formation of Antibody-Biotin-Streptavidin NanoBEADS (ABS NanoBEADS) using 165 ± 11 nm diameter NPs. Informed by our prior work, (Suh et al., 2018b) all NanoBEADS assembly experiments were conducted at the bacteria to NPs ratio 1:100 and biotinylated antibody concentration of $10 \mu\text{g}/\text{mL}$ (see Methods for detail). The number of attached NPs on each bacterium was quantified using Scanning Electron Microscopy (SEM) and reported as the number of attached NPs per projected unit area of the cell surface ($\#\text{NPs}/\mu\text{m}^2$).

We first evaluated the effect of assembly volume and duration using a vortex mixer (V) for two different assembly volumes of $100 \mu\text{L}$ (V-100) and $800 \mu\text{L}$ (V-800) and three different assembly periods of 30, 60, and 90 min. As shown in **Figure 3a**, assembly volume had no statistically significant effect on the average NP attachment density of ABS NanoBEADS constructed using a vortex mixer, except for the significantly decreased NPs attachment density in the 60 min assembly period, when the volume increased from $100 \mu\text{L}$ to $800 \mu\text{L}$ ($p < 0.01$). In the case of $100 \mu\text{L}$ assembly volume, the NPs attachment density significantly increased by increasing duration from 30 min to 60 min ($p < 0.01$). In contrast, there was no significant difference in the NPs attachment density for V-800-60 comparing to the other two durations of V-800, as shown in Figure 3a, b. Keeping the high throughput biofabrication needs for in vivo experiments and future translational applications in mind, we examined other mixing methods at the higher $800 \mu\text{L}$ volume and compared the results from V-800 with those of the Belly Dancer[®] mixer (B-800) and the end-over-end mixer (E-800) for each of the three assembly durations. For all the assembly periods tested, the Belly Dancer[®] and the

Mixing Method	Speed (rpm)	Assembly Volume (μL)	Assembly Period (min)
Vortex mixer (V)	500	100	30, 60, 90
Vortex mixer (V)	500	800	30, 60, 90
Belly Dancer [®] mixer (B)	100	800	30, 60, 90
End-over-end mixer (E)	15	800	30, 60, 90

Table 1: Table of assembly process parameters (see Methods for details).

end-over-end mixer resulted in similar or higher average NPs areal density, compared to the vortex mixer (Figure 3a). For the former two mixing methods, as the assembly period increased from 30 min to 60 min, the count of NanoBEADS with attachment numbers higher than $10 \text{ NPs}/\mu\text{m}^2$ cell area showed an appreciable increase while the number of bacteria without any NP attached ($0 \text{ NPs}/\mu\text{m}^2$) decreased (Figure 3c,d). Upon increasing the assembly time to 90 min, more NanoBEADS with attachment density lower than $10 \text{ NPs}/\mu\text{m}^2$ were observed (Figure 3c,d), resulting in an overall decrease in average attachment density (Figure 3a). This reduction in attachment density can be attributable to the presence of residual culture media in the assembly volume, which led to some bacteria growth during the more extended assembly period. Therefore, 60 min was identified as the optimal assembly duration. B-800-60 and E-800-60 cases had significantly higher NPs attachment density than V-800-60 case ($p < 0.05$). Additionally, there was a significant difference in the NPs attachment density in E-800-60 comparing to the other two durations ($p < 0.01$). Moreover, the E-800-60 case had a statistically significant higher average NP attachment density than the NanoBEADS constructed using a vortex mixer, except for the V-100-60 case, where the difference was not statistically significant. Altogether, our results suggest that the Belly Dancer[®] mixer used with $800 \mu\text{L}$ assembly volume for 60 min (B-800-60), and the end-over-end mixer used with $800 \mu\text{L}$ assembly volume for 60 mins (E-800-60) were the optimal sets of assembly parameters, among the combinations tested.

Effect of the linkage chemistry on areal density and repeatability of NP attachment

Due to the stochastic nature of the assembly process, a distribution of the particle attachment density is expected for each individual experiment, as shown in Figure 3. However, minimizing the variance in NP

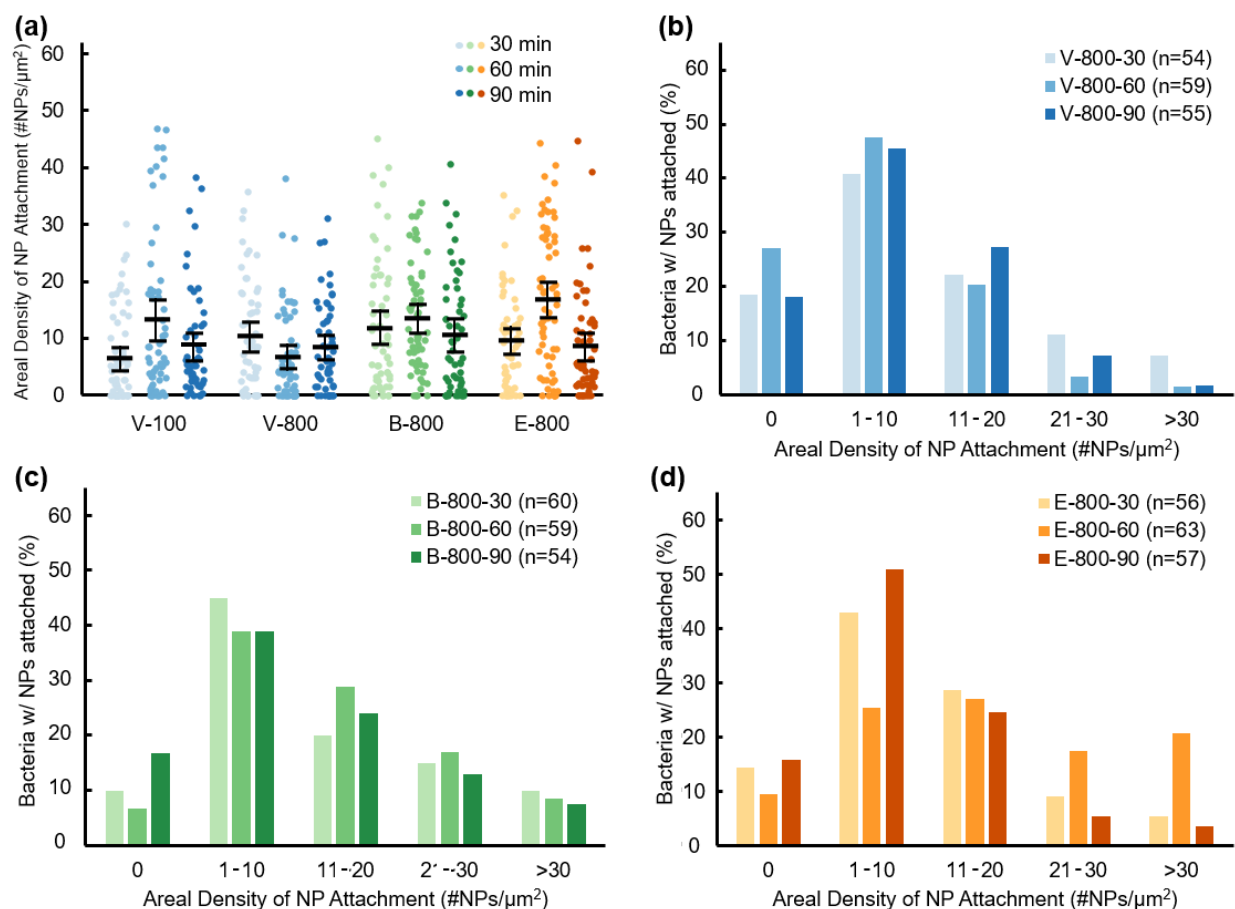


Figure 3: Effect of assembly process parameters on 165 nm diameter nanoparticle (NP) attachment density in Antibody-Biotin-Streptavidin NanoBEADS (ABS NanoBEADS). (a) Effect of mixing method, assembly volume, and assembly duration on the attached NP areal density. The black bars indicate means and 95% confidence intervals (i.e., nonoverlapping bars between any two cases indicate a significant difference with a p -value < 0.05). Effect of assembly period on the distribution of the attached NP areal density for (b) V-800, (c) B-800, and (d) E-800. In all plot legends, X-000-00 denote the mixing method (X), assembly volume (000), and assembly period (00), as described in Table 1. All areal densities are calculated based on projected cell area.

cargo attachment density distribution across replicate experiments is crucial to determining the efficacious dosage of biohybrid systems towards robust and predictable therapeutic outcomes. Thus, we next examined the repeatability in NP attachment density outcomes for two linkage chemistries using the optimal assembly parameters of B-800-60 and E-800-60. In both NanoBEADS variants, streptavidin-coated nanoparticles were attached to the bacteria using the high affinity biotin-streptavidin interactions; however, in the ABS NanoBEADS variant, biotin was conjugated with anti-Salmonella antibody and covalently bonded to the antigen on bacteria, whereas in the Biotin-Streptavidin NanoBEADS (BS NanoBEADS) variant, biotin was adsorbed onto the bacteria via electrostatic interactions. A minimum of four independent replicate assembly experiments for each of the two NanoBEADS variants were conducted (**Figure 4**). For the ABS NanoBEADS, both B-800-60 and E-800-60 yielded similar results (Figures 3a, b), with E-800-60 producing a higher fraction of high NP density NanoBEADS (> 20 $\#NPs/\mu m^2$) (Figure 3c) and a more repeatable attachment density distribution with a smaller variance (Figure 3d). Thus, we identify E-800-60 as the

optimal set of assembly parameters for producing the ABS NanoBEADS. For the BS NanoBEADS, no significant difference between the B-800-60 and E-800-60 outcomes was observed (Figure 4e, f). Comparing the distribution of the attached NP areal density between the two variants (Figures 4c, g), it is evident that the ABS NanoBEADS had a significantly higher number of bacteria with greater attachment density than the BS NanoBEADS. Furthermore, only ~7% of the bacteria did not have any nanoparticle attached when the ABS linkage is used, whereas an average of ~27% did not have any NP attached when the BS linkage is used. Consistent with our observation for ABS NanoBEADS, E-800-60 produced a more repeatable attachment density distribution (Figure 4h). The viability of the bacteria was not affected by the attached NPs in either of the two variants (**Figure S1**).

Effect of NP size on attachment density and growth rate

Next, we investigated the effect of particle size on the attachment density outcome in the ABS and BS NanoBEADS variants constructed using the optimal assembly parameters of E-800-60 and 165 ± 11 nm or 121 ± 6 nm particles. Representative scanning electron microscopy (SEM) images of both NanoBEADS variants are shown in Figure 5a-d. As shown in Figure 5e, NPs with a smaller diameter of 121 ± 6 nm had significantly increased attachment density ($p < 0.0001$) for ABS NanoBEADS, but the slightly increased attachment density for BS NanoBEADS was not statistically significant. Consistent with our observation of NanoBEADS constructed with large NPs, there was an average of 70% decrease in the NP areal density upon changing from the ABS linkage chemistry to the antibody-free BS linkage chemistry (Figure 5e). Our results suggest that irrespective of NP size, the linkage chemistry (i.e., the method used to present biotin on the bacteria outer membrane) significantly affects the NP attachment outcome. When the biotinylated antibody is used, more particles per bacteria are attached compared to using physisorbed biotin. The observed trends in the effect of NP size on the NP attachment density were conserved when the closely comparable B-800-60 assembly parameters were used (**Figure S3a**).

We next examined the effect of NP size and attachment density on the growth of NanoBEADS. While NanoBEADS can be stored in media that do not support growth *in vitro*, they are expected to operate *in vivo* for days (Suh et al., 2019) and are observed to grow in the nutrient-rich tumor microenvironment. (Suh et al., 2018a) As NanoBEADS grow, the attached NP load is divided amongst the daughter cells, leading to a more effective distribution of the NPs within the tumor. (Suh et al., 2019) Furthermore, many tumor-targeting bacteria, including *S. Typhimurium* VNP20009 used in this study, have instinct and immune-mediated antitumor effects (Song et al., 2018) (Zhou et al., 2018) in addition to serving as a delivery vector for the nanomedicine attached to their outer membrane. Thus, intratumoral bacterial growth augments the therapeutic effect of fixed nanomedicine payload. The doubling times of both NanoBEADS variants at both NP sizes were measured and compared to the doubling time of the bacteria (control). All experiments were performed in a mammalian cell culture medium, given the ultimate application of the NanoBEADS platform as a cancer drug delivery system. For the optimal assembly parameters, i.e., E-800-60, we first investigated if coating of the outer membrane or the mechanical agitation of the assembly process affects the growth rate. We found no statistically significant difference in the average doubling time of unmodified bacteria, biotinylated antibody-coated bacteria, and biotin-coated (physisorbed) bacteria, suggesting that surface modification did not affect the bacterial growth rate (**Figure S2**). However, bacteria subjected to mechanical agitation experienced during the E-800-60 assembly process (in the absence of NPs) resulted in a statistically significant ($p < 0.05$) increase in the average doubling time of the bacteria from 49 ± 3 min to 59 ± 4 min, which may be attributable to the mechanical stress. Next, we measured the doubling time of the NanoBEADS constructs and compared them to the doubling time of the mechanically-treated (E-800-60) bacteria as the baseline control (Figure 5f). The average doubling time of the 165 nm and 121 nm ABS NanoBEADS were 95 ± 8 min and 104 ± 2 min, both of which were significantly longer ($p < 0.05$) than the control doubling time. The average doubling time of the 165 nm and 121 nm BS NanoBEADS were significantly shorter ($p < 0.05$) than their ABS NanoBEADS counterparts at 64 ± 0.2 min and 54 ± 5 min. Interestingly, no significant difference between the doubling time of BS NanoBEADS and control bacteria was observed. We attribute the significantly longer doubling time of the ABS NanoBEADS ($p < 0.05$) to the higher

NP attachment areal density, as shown in Figure 5a. NP size did not significantly affect the NanoBEADS doubling time within each variant type ($p > 0.05$). Altogether, our results suggest that NP attachment density and not the NP size affects the NanoBEADS doubling time for the range of NP size tested. The observed trend in the effect of NP size on growth rate was conserved when the closely comparable B-800-60 assembly parameters were used (Figure S3b). Lastly, we note that the dependency of doubling time on NP attachment density may become less significant with particle size reduction. We observed that the doubling time of the ABS NanoBEADS constructed with significantly smaller 40 nm gold particles at comparable NP attachment density to 165 nm PLGA particles was comparable to that of control (**Figure S4, S5**).

Effect of NP size and attachment density on NanoBEADS motility

We next assessed the effect of NP size and attachment density on motility by measuring each NanoBEADS variant's swimming speeds with small or large NP attached and compared the speeds with that of bacteria as the baseline (control). Before characterizing NanoBEADS motile behavior, we first evaluated how chemical and mechanical processes that comprise the NanoBEADS construction process affect the bacteria motility in the absence of NPs. The average speeds of the bacteria cultured under standard microbiological conditions (control), mechanically-treated bacteria without antibody coating or nanoparticle attachment (control, E-800-60), antibody-coated bacteria, and mechanically-treated (E-800-60) antibody-coated bacteria without particles are shown in **Figure 6a**. Mechanical agitation decreased the average speed of bacteria from 9.2 ± 5.6 $\mu\text{m/s}$ to 4.8 ± 3.9 $\mu\text{m/s}$ ($p < 0.05$). However, the choice of mixing method did not have a statistically significant effect on the bacteria motility speed (Figure S3c). Antibody coating of bacteria had a similar statistically significant reducing effect on the bacteria motility speed to 4.5 ± 1.5 $\mu\text{m/s}$ ($p < 0.05$). The combination of mechanical agitation and antibody coating did not result in any further statistically significant degradation in speed (4.7 ± 2.1 $\mu\text{m/s}$). We attribute the reduction in swimming speed to the fragile structure of the flagella in *S. Typhimurium* VNP20009 cheY+, which can be disrupted through mechanical agitation. ([Broadway et al., 2017](#))

We next examined the motility speed of both NanoBEADS variants constructed using the E-800-60 assembly parameters and attached with 165 nm or 121 nm NPs, as shown in Figure 6b and S3d. To assess the effect of NP size, we compared the motility speed within each variant category. We did not observe a statistically significant difference between the 121 nm ABS NanoBEADS average swimming speed (4.4 ± 1.0 $\mu\text{m/s}$) and the 165 nm ABS NanoBEADS (4.0 ± 1.2 $\mu\text{m/s}$). It appears that the contribution of the larger 165 nm NPs to the drag force is comparable to the contribution of the larger quantity of the smaller 121 nm particles (Figure 5e). In the case of BS NanoBEADS, the NanoBEADS with the smaller 121 nm NPs have a lower average speed (4.2 ± 0.5 $\mu\text{m/s}$) than NanoBEADS with 165 nm NPs (4.5 ± 1.4 $\mu\text{m/s}$), but the difference is not statistically significant. To assess the effect of linkage chemistry on motility speed, we compared the motility speed of the two NanoBEADS variants at each particle size. In the case of NanoBEADS with 165 nm NPs, BS NanoBEADS have a significantly higher average speed than ABS NanoBEADS ($p < 0.01$), presumably due to the lower NP attachment density. Whereas, for the NanoBEADS with the smaller 121 nm NPs, both NanoBEADS variants have similar average speed, which was not significantly different from the average speed of antibody-coated E-800-60 control bacteria.

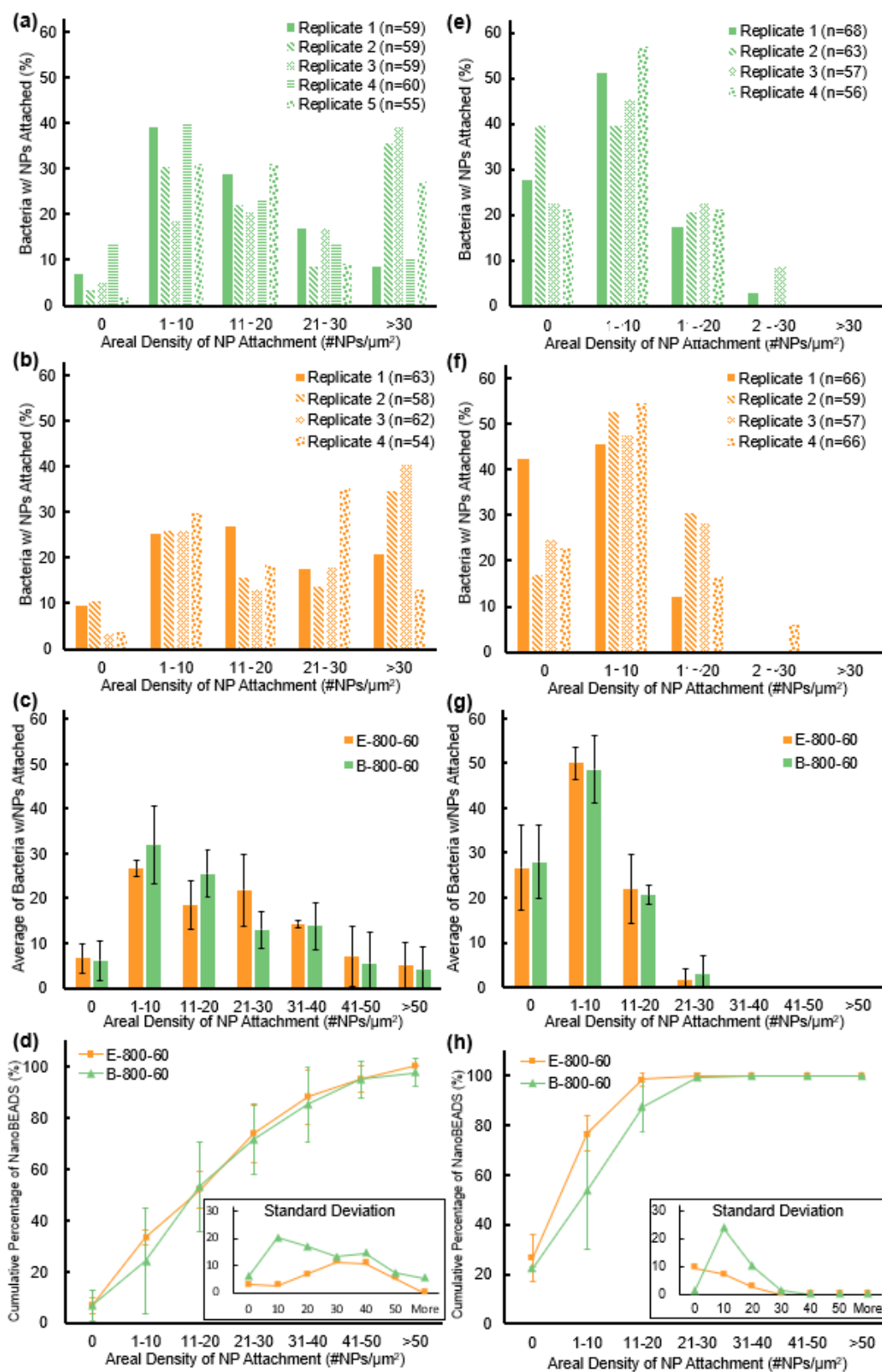


Figure 4: Effect of mixing method and linkage chemistry on the areal density and repeatability of nanoparticle (NP) attachment. Repeatability of NP attachment areal density distribution for Antibody-Biotin-Streptavidin NanoBEADS (ABS NanoBEADS) constructed using the process parameters of (a) B-800-60 and (b) E-800-60, and for Biotin-Streptavidin NanoBEADS (BS NanoBEADS) constructed using process parameters of (e) B-800-60 and (f) E-800-60. Average NP attachment areal density distribution for (c) ABS NanoBEADS and (g) BS NanoBEADS constructed using the process parameters of B-800-60 and E-800-60. Cumulative percentage of NanoBEADS and standard deviation as a function of NP areal density (inset) for (d) ABS NanoBEADS and (h) BS NanoBEADS constructed using the process parameters of B-800-60

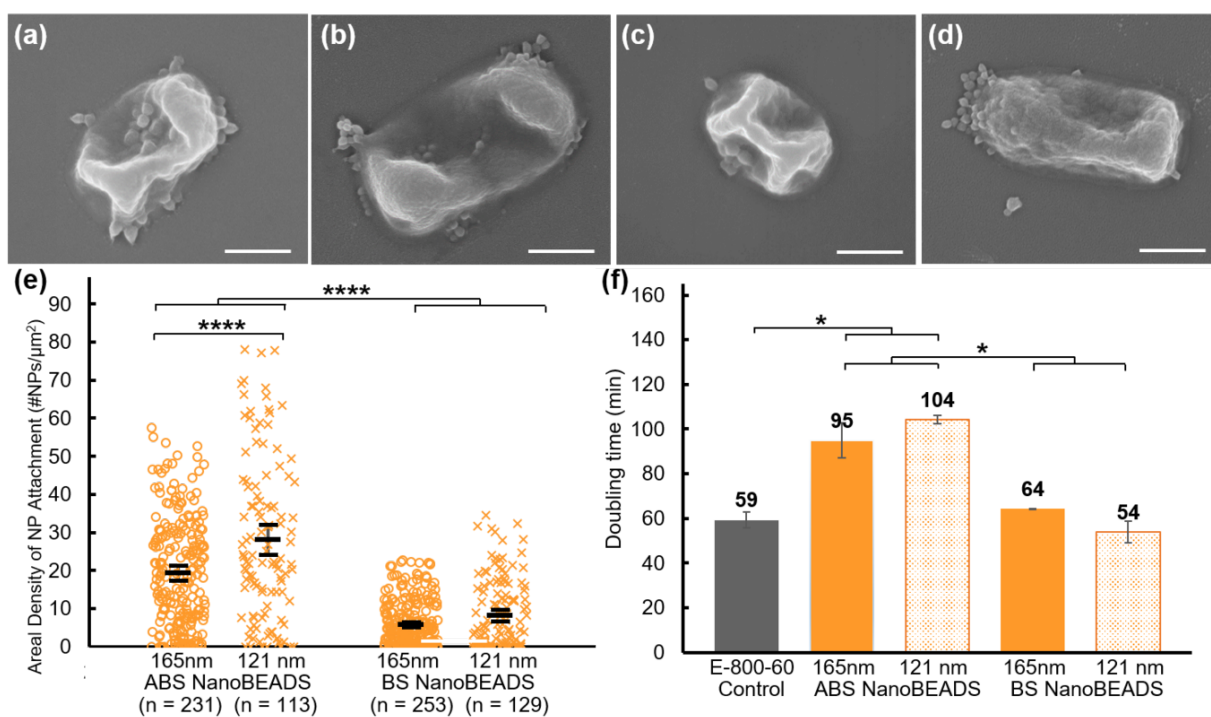


Figure 5: Effect of nanoparticle (NP) size and linkage chemistry on attachment density and growth rate. Representative scanning electron microscopy (SEM) images of (a) ABS NanoBEADS (E-800-60) with 165 nm NPs, (b) ABS NanoBEADS (E-800-60) with 121 nm NPs, (c) BS NanoBEADS (E-800-60) with 165 nm NPs, (d) BS NanoBEADS (E-800-60) with 121 nm NPs. All scale bars are 500 nm. (e) The NP areal attachment density as a function of NP size for the ABS NanoBEADS and BS NanoBEADS variants. The black bars indicate means and 95% confidence intervals. ****p-value < 0.0001. (f) The comparison of doubling time of the variants of NanoBEADS and mechanically-treated (E-800-60) bacteria with no particles attached as the control. Each data point represents the mean \pm standard deviation. *p-value < 0.05.

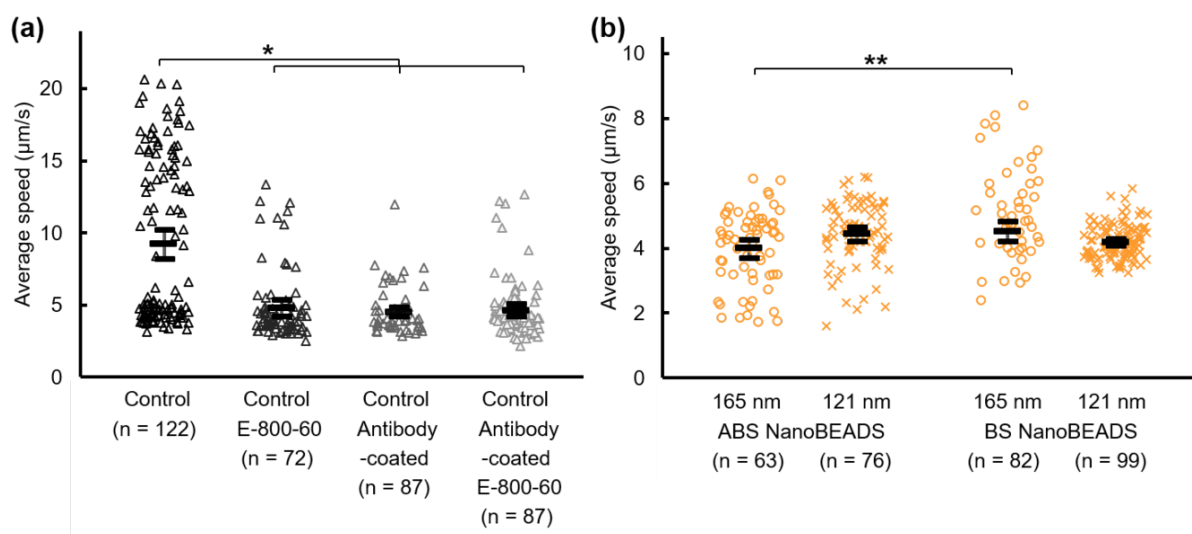


Figure 6: Effect of nanoparticle (NP) size, quantity, and linkage chemistry on NanoBEADS motility speed. (a) The effect of mixing-induced shear and antibody coating on the average speed of bacteria (without NPs) at 2 hr incubation time. (b) The average speed of the ABS and BS NanoBEADS constructed using small or large NPs at 2 hr incubation time. In both plots, the black bars indicated means and 95% confidence intervals. *p-value < 0.05; **p-value < 0.01.

Conclusion

The NanoBEADS is a bacteria-based bio-hybrid drug delivery system designed to utilize self-propelling motile bacteria to enhance the interstitial delivery of nanomedicine. As is the case for all biohybrid delivery systems, the effectiveness of NanoBEADS hinges upon maximizing its NP load without affecting its viability and minimal effect on its motility. It is also imperative that the NanoBEADS construction process produces a repeatable distribution of NP load densities (i.e., therapeutic load) to facilitate the use of such a system in translational applications. Thus, a systematic investigation of the effects of the assembly process parameters, linkage chemistry, and NP size on NanoBEADS properties (i.e., NP attachment density and repeatability, growth rate, and swimming speed) was carried out. We selected biotin-streptavidin linkage chemistry for this study due to its prevalence in constructing bacteria-based biohybrid microrobots (Akin et al., 2007)(Traore et al., 2014)(Kazmierczak et al., 2014)(Nguyen et al., 2016)(Alapan et al., 2018)(Kojima et al., 2012)(Huter et al., 1999)(Buss et al., 2020)(Hiratsuka et al., 2005)(Singh et al., 2017)(Carlsen et al., 2014). Furthermore, the peritrichously flagellated *S. Typhimurium* was selected due to the common use of Gram-negative bacteria (*E. coli*, *S. marcescens*, etc.) as well as other flagellated bacteria in the construction of bacteria-based microrobots. The selected PLGA nanoparticles of two different sizes represent a good model for the polymeric nanoparticles used in constructing biohybrid microrobots. For the ABS NanoBEADS, using an end-over-end mixer with a total mixing volume of 800 μL for 60 min assembly period (E-800-60) produced the highest and most repeatable NP attachment density without affecting the viability of the bacteria. In the case of BS NanoBEADS, where streptavidin-functionalized nanoparticles were attached to the bacteria using biotin that was physisorbed to the bacteria, the attachment density decreased by more than 70%, compared to the ABS NanoBEADS case. The optimal NanoBEADS construction strategy reported herein is extensible to other NP materials and sizes (Figure S4). The motility speed is adversely affected with the attachment of larger particles at high density, but the attachment of NPs smaller than 120 nm did not affect the motility speed even at high attachment density (Figure S4). Irrespective of NP size, reduction in attachment density restored the growth rate to the control bacteria levels. However, growth was unaffected for the smaller 40 nm gold NPs even at the high NP attachment density of 21 gold NPs/ μm^2 (Figure S5).

Altogether, we posit that the new knowledge in the effect of assembly parameters and linkage chemistry on bacteria-nanoparticle assembly outcomes and the effect of NP size on key bacterial behaviors of motility and growth in bacteria-based biohybrid systems will facilitate the design and development of more efficacious bacteria-mediated delivery systems for a variety of applications. The exact quantitative values for attachment density or changes in motility speed and growth rate are likely to depend on the choice of bacteria, nanoparticle, and linkage chemistry. Nonetheless, the observed trends, such as the effect of assembly parameters on nanoparticle attachment density and repeatability, are expected to be generalizable (Figure S5). Similarly, the reported trends for the effect of linkage chemistry on nanoparticle attachment density or the effect of nanoparticle size and density on motility speed and growth rate can inform the design of process parameters and nanoparticle selection in other bacteria-based biohybrid systems.

Acknowledgements

This project was partially supported by the National Science Foundation (CAREER award, CBET-1454226) and the Institute for Critical Technology and Applied Science (ICTAS) at Virginia Tech.

Supporting Information

Supporting Information is available from the Wiley Online Library.



Figure 7: Schematic of the Antibody-Biotin-Streptavidin NanoBEADS (ABS NanoBEADS).

References

- J. Adler. Chemotaxis in Bacteria. *Science*, 153(3737):708–716, aug 1966. doi: 10.1126/science.153.3737.708. URL <https://doi.org/10.1126%2Fscience.153.3737.708>.
- Demir Akin, Jennifer Sturgis, Kathy Ragheb, Debby Sherman, Kristin Burkholder, J. Paul. Robinson, Arun K. Bhunia, Sulma Mohammed, and Rashid Bashir. Bacteria-mediated delivery of nanoparticles and cargo into cells. *Nature Nanotechnology*, 2(7):441–449, jun 2007. doi: 10.1038/nnano.2007.149. URL <https://doi.org/10.1038%2Fnnano.2007.149>.
- Yunus Alapan, Oncay Yasa, Oliver Schauer, Joshua Giltinan, Ahmet F. Tabak, Victor Sourjik, and Metin Sitti. Soft erythrocyte-based bacterial microswimmers for cargo delivery. *Science Robotics*, 3(17):eaar4423, apr 2018. doi: 10.1126/scirobotics.aar4423. URL <https://doi.org/10.1126%2Fscirobotics.aar4423>.

- J Bastos-Arrieta, A Revilla-Guarinos, WE Uspal, and J Simmchen. Bacterial Biohybrid Microswimmers. *Front Robot AI*, 5:97, 2018.
- Partha Basu, Ajay Mehta, Minish Jain, Sudeep Gupta, Rajnish V. Nagarkar, Subhashini John, and Robert Petit. A Randomized Phase 2 Study of ADXS11-001 *Listeria monocytogenes*-Listeriolysin O Immunotherapy With or Without Cisplatin in Treatment of Advanced Cervical Cancer. *International Journal of Gynecologic Cancer*, 28(4):764–772, may 2018. doi: 10.1097/igc.0000000000001235. URL <https://doi.org/10.1097%2Ffigc.0000000000001235>.
- Bahareh Behkam and Metin Sitti. Effect of quantity and configuration of attached bacteria on bacterial propulsion of microbeads. *Applied Physics Letters*, 93(22):223901, dec 2008. doi: 10.1063/1.3040318. URL <https://doi.org/10.1063%2F1.3040318>.
- Devaki Bhaya. Light matters: phototaxis and signal transduction in unicellular cyanobacteria. *Molecular Microbiology*, 53(3):745–754, jun 2004. doi: 10.1111/j.1365-2958.2004.04160.x. URL <https://doi.org/10.1111%2Fj.1365-2958.2004.04160.x>.
- Katherine M. Broadway, Seungbeum Suh, Bahareh Behkam, and Birgit E. Scharf. Optimizing the restored chemotactic behavior of anticancer agent *Salmonella enterica* serovar Typhimurium VNP20009. *Journal of Biotechnology*, 251:76–83, jun 2017. doi: 10.1016/j.jbiotec.2017.04.006. URL <https://doi.org/10.1016%2Fj.jbiotec.2017.04.006>.
- N Buss, O Yasa, Y Alapan, MB Akolpoglu, and M Sitti. Nanoerythrocyte-functionalized biohybrid microswimmers. *APL Bioeng*, 4:026103, Jun 2020.
- RW Carlsen, MR Edwards, J Zhuang, C Pacoret, and M Sitti. Magnetic steering control of multi-cellular bio-hybrid microswimmers. *Lab Chip*, 14:3850–9, Oct 2014.
- JP Celli, BS Turner, NH Afdhal, S Keates, I Ghiran, CP Kelly, RH Ewoldt, GH McKinley, P So, S Erramilli, and R Bansil. *Helicobacter pylori* moves through mucus by reducing mucin viscoelasticity. *Proc Natl Acad Sci U S A*, 106:14321–6, Aug 2009.
- Mi-Ran Choi, Katie J. Stanton-Maxey, Jennifer K. Stanley, Carly S. Levin, Rizia Bardhan, Demir Akin, Sunil Badve, Jennifer Sturgis, J. Paul Robinson, Rashid Bashir, Naomi J. Halas, and Susan E. Clare. A Cellular Trojan Horse for Delivery of Therapeutic Nanoparticles into Tumors. *Nano Letters*, 7(12): 3759–3765, dec 2007. doi: 10.1021/nl072209h. URL <https://doi.org/10.1021%2Fn1072209h>.
- C. Clairmont, K. C. Lee, J. Pike, M. Ittensohn, K. B. Low, J. Pawelek, D. Bermudes, S. M. Brecher, D. Margitich, J. Turnier, Z. Li, X. Luo, I. King, and L. M. Zheng. Biodistribution and Genetic Stability of the Novel Antitumor Agent VNP20009 a Genetically Modified Strain of *Salmonella typhimurium*. *The Journal of Infectious Diseases*, 181(6):1996–2002, jun 2000. doi: 10.1086/315497. URL <https://doi.org/10.1086%2F315497>.
- Damien Faivre and Dirk Schüler. Magnetotactic Bacteria and Magnetosomes. *Chemical Reviews*, 108(11): 4875–4898, oct 2008. doi: 10.1021/cr078258w. URL <https://doi.org/10.1021%2Fcr078258w>.
- Ouajdi Felfoul, Mahmood Mohammadi, Samira Taherkhani, Dominic de Lanauze, Yong Zhong Xu, Dumitru Loghin, Sherief Essa, Sylwia Jancik, Daniel Houle, Michel Lafleur, Louis Gaboury, Maryam Tabrizian, Neila Kaou, Michael Atkin, Té Vuong, Gerald Batist, Nicole Beauchemin, Danuta Radzioch, and Sylvain Martel. Magneto-aerotactic bacteria deliver drug-containing nanoliposomes to tumour hypoxic regions. *Nature Nanotechnology*, 11(11):941–947, aug 2016. doi: 10.1038/nnano.2016.137. URL <https://doi.org/10.1038%2Fnnano.2016.137>.
- S Gekle. Strongly Accelerated Margination of Active Particles in Blood Flow. *Biophys J*, 110:514–520, Jan 2016.
- David M. Heimann and Steven A. Rosenberg. Continuous Intravenous Administration of Live Genetically Modified *Salmonella Typhimurium* in Patients With Metastatic Melanoma. *Journal of Immunotherapy*,

26(2):179–180, mar 2003. doi: 10.1097/00002371-200303000-00011. URL <https://doi.org/10.1097/2F00002371-200303000-00011>.

Y Hiratsuka, M Miyata, and TQ Uyeda. Living microtransporter by uni-directional gliding of Mycoplasma along microtracks. *Biochem Biophys Res Commun*, 331:318–24, May 2005.

Bonnie Huang, Wuhbet D. Abraham, Yiran Zheng, Sandra C. Bustamante López, Samantha S. Luo, and Darrell J. Irvine. Active targeting of chemotherapy to disseminated tumors using nanoparticle-carrying T cells. *Science Translational Medicine*, 7(291):291ra94–291ra94, jun 2015. doi: 10.1126/scitranslmed.aaa5447. URL <https://doi.org/10.1126/2Fscitranslmed.aaa5447>.

V Huter, MP Szostak, J Gampfer, S Prethaler, G Wanner, F Gabor, and W Lubitz. Bacterial ghosts as drug carrier and targeting vehicles. *J Control Release*, 61:51–63, Aug 1999.

Robert Kazmierczak, Elizabeth Choe, Jared Sinclair, and Abraham Eisenstark. Direct Attachment of Nanoparticle Cargo to Salmonella typhimurium Membranes Designed for Combination Bacteriotherapy Against Tumors. In *Methods in Molecular Biology*, pages 151–163. Springer New York, sep 2014. doi: 10.1007/978-1-4939-1625-2_11. URL https://doi.org/10.1007/2F978-1-4939-1625-2_11.

M Kihara and R M Macnab. Cytoplasmic pH mediates pH taxis and weak-acid repellent taxis of bacteria. *Journal of Bacteriology*, 145(3):1209–1221, mar 1981. doi: 10.1128/jb.145.3.1209-1221.1981. URL <https://doi.org/10.1128/2Fjb.145.3.1209-1221.1981>.

Masaru Kojima, Zhenhai Zhang, Masahiro Nakajima, and Toshio Fukuda. High efficiency motility of bacteria-driven liposome with raft domain binding method. *Biomedical Microdevices*, 14(6):1027–1032, sep 2012. doi: 10.1007/s10544-012-9711-2. URL <https://doi.org/10.1007/2Fs10544-012-9711-2>.

Dung T. Le, Thomas W. Dubensky, and Dirk G. Brockstedt. Clinical Development of Listeria monocytogenes–Based Immunotherapies. *Seminars in Oncology*, 39(3):311–322, jun 2012. doi: 10.1053/j.seminoncol.2012.02.008. URL <https://doi.org/10.1053/2Fj.seminoncol.2012.02.008>.

Dung T. Le, Andrea Wang-Gillam, Vincent Picozzi, Tim F. Greten, Todd Crocenzi, Gregory Springett, Michael Morse, Herbert Zeh, Deirdre Cohen, Robert L. Fine, Beth Onners, Jennifer N. Uram, Daniel A. Laheru, Eric R. Lutz, Sara Solt, Aimee Luck Murphy, Justin Skoble, Ed Lemmens, John Grous, Thomas Dubensky, Dirk G. Brockstedt, and Elizabeth M. Jaffee. Safety and Survival With GVAX Pancreas Prime and Listeria Monocytogenes–Expressing Mesothelin (CRS-207) Boost Vaccines for Metastatic Pancreatic Cancer. *Journal of Clinical Oncology*, 33(12):1325–1333, apr 2015. doi: 10.1200/jco.2014.57.4244. URL <https://doi.org/10.1200/2Fjco.2014.57.4244>.

K. Brooks Low, Martina Ittensohn, Trung Le, James Platt, Stefano Sodi, Max Amoss, Olivia Ash, Ellen Carmichael, Ashok Chakraborty, Jessica Fischer, Stanley L. Lin, Xi-ang Luo, Samuel I. Miller, Li mou Zheng, Ivan King, John M. Pawelek, and David Bermudes*. *Lipid Amutant Salmonella with suppressed virulence and TNF induction retain tumor – targeting in vivo*. *Nature Biotechnology*, 17(1) : 37 – –41, jan 1999. doi : . URL <https://doi.org/10.1038/2F5205>.

Rachael Mooney, Luella Roma, Donghong Zhao, Desiree Van Haute, Elizabeth Garcia, Seung U. Kim, Alexander J. Annala, Karen S. Aboody, and Jacob M. Berlin. Neural Stem Cell-Mediated Intratumoral Delivery of Gold Nanorods Improves Photothermal Therapy. *ACS Nano*, 8(12):12450–12460, nov 2014. 10.1021/nn505147w. URL <https://doi.org/10.1021/2Fnn505147w>.

John Nemunaitis, Casey Cunningham, Neil Senzer, Joseph Kuhn, Jennifer Cramm, Craig Litz, Robert Cavagnolo, Ann Cahill, Caroline Clairmont, and Mario Sznol. Pilot trial of genetically modified attenuated Salmonella expressing the E. coli cytosine deaminase gene in refractory cancer patients. *Cancer Gene Therapy*, 10(10):737–744, sep 2003. 10.1038/sj.cgt.7700634. URL <https://doi.org/10.1038/2Fs.cgt.7700634>.

Van Du Nguyen, Ji-Won Han, Young Jin Choi, Sunghoon Cho, Shaohui Zheng, Seong Young Ko, Jong-Oh Park, and Sukho Park. Active tumor-therapeutic liposomal bacteriobot combining a drug (paclitaxel)-encapsulated liposome with targeting bacteria (*Salmonella Typhimurium*). *Sensors and Actuators B: Chemical*, 224:217–224, mar 2016. 10.1016/j.snb.2015.09.034. URL <https://doi.org/10.1016%2Fj.snb.2015.09.034>.

N. J. Roberts, L. Zhang, F. Janku, A. Collins, R.-Y. Bai, V. Staedtke, A. W. Rusk, D. Tung, M. Miller, J. Roix, K. V. Khanna, R. Murthy, R. S. Benjamin, T. Helgason, A. D. Szvalb, J. E. Bird, S. Roy-Chowdhuri, H. H. Zhang, Y. Qiao, B. Karim, J. McDaniel, A. Elpiner, A. Sahora, J. Lachowicz, B. Phillips, A. Turner, M. K. Klein, G. Post, L. A. Diaz, G. J. Riggins, N. Papadopoulos, K. W. Kinzler, B. Vogelstein, C. Bettegowda, D. L. Huso, M. Varterasian, S. Saha, and S. Zhou. Intratumoral injection of *Clostridium novyi*-NT spores induces antitumor responses. *Science Translational Medicine*, 6(249):249ra111–249ra111, aug 2014. 10.1126/scitranslmed.3008982. URL <https://doi.org/10.1126%2Fscitranslmed.3008982>.

Mathilde Roger, Anne Clavreul, Marie-Claire Venier-Julienne, Catherine Passirani, Laurence Sindji, Paul Schiller, Claudia Montero-Menei, and Philippe Menei. Mesenchymal stem cells as cellular vehicles for delivery of nanoparticles to brain tumors. *Biomaterials*, 31(32):8393–8401, nov 2010. 10.1016/j.biomaterials.2010.07.048. URL <https://doi.org/10.1016%2Fj.biomaterials.2010.07.048>.

Christine K. Schmidt, Mariana Medina-Sánchez, Richard J. Edmondson, and Oliver G. Schmidt. Engineering microrobots for targeted cancer therapies from a medical perspective. *Nature Communications*, 11(1), nov 2020. 10.1038/s41467-020-19322-7. URL <https://doi.org/10.1038%2Fs41467-020-19322-7>.

Friedrich H. Schmitz-Winnenthal, Nicolas Hohmann, Thomas Schmidt, Lilli Podola, Tobias Friedrich, Heinz Lubenau, Marco Springer, Sébastien Wieckowski, Klaus M. Breiner, Gerd Mikus, Markus W. Büchler, Anne-Valerie Keller, Ruhan Koc, Christoph Springfeld, Phillip Knebel, Mariana Bucur, Lars Grenacher, Walter E. Haefeli, and Philipp Beckhove. A phase 1 trial extension to assess immunologic efficacy and safety of prime-boost vaccination with VXM01 an oral T cell vaccine against VEGFR2, in patients with advanced pancreatic cancer. *OncoImmunology*, 7(4):e1303584, jan 2018. 10.1080/2162402x.2017.1303584. URL <https://doi.org/10.1080%2F2162402x.2017.1303584>.

AV Singh, Z Hosseinidoust, BW Park, O Yasa, and M Sitti. Microemulsion-Based Soft Bacteria-Driven Microswimmers for Active Cargo Delivery. *ACS Nano*, 11:9759–9769, Oct 2017.

S Song, MS Vuai, and M Zhong. The role of bacteria in cancer therapy - enemies in the past, but allies at present. *Infect Agent Cancer*, 13:9, 2018.

Matthias T Stephan, James J Moon, Soong Ho Um, Anna Bershteyn, and Darrell J Irvine. Therapeutic cell engineering with surface-conjugated synthetic nanoparticles. *Nature Medicine*, 16(9):1035–1041, aug 2010. 10.1038/nm.2198. URL <https://doi.org/10.1038%2Fnm.2198>.

S Suh, EJ Leaman, Y Zhan, and B Behkam. Mathematical Modeling of Bacteria-Enabled Drug Delivery System Penetration into Multicellular Tumor Spheroids. *Annu Int Conf IEEE Eng Med Biol Soc*, 2018: 6162–6165, Jul 2018a.

S Suh, A Jo, MA Traore, Y Zhan, SL Coutermarsh-Ott, VM Ringel-Scaia, IC Allen, RM Davis, and B Behkam. Nanoscale Bacteria-Enabled Autonomous Drug Delivery System (NanoBEADS) Enhances Intratumoral Transport of Nanomedicine. *Adv Sci (Weinh)*, 6:1801309, Feb 2019.

SeungBeum Suh, Ami Jo, Mahama A. Traore, Ying Zhan, Sheryl L. Coutermarsh-Ott, Veronica M. Ringel-Scaia, Irving C. Allen, Richey M. Davis, and Bahareh Behkam. Nanoscale Bacteria-Enabled Autonomous Drug Delivery System (NanoBEADS) Enhances Intratumoral Transport of Nanomedicine. *Advanced Science*, 6(3):1801309, dec 2018b. 10.1002/advs.201801309. URL <https://doi.org/10.1002%2Fadvs.201801309>.

Samira Taherkhani, Mahmood Mohammadi, Jamal Daoud, Sylvain Martel, and Maryam Tabrizian. Covalent Binding of Nanoliposomes to the Surface of Magnetotactic Bacteria for the Synthesis of Self-

Propelled Therapeutic Agents. *ACS Nano*, 8(5):5049–5060, apr 2014. 10.1021/nm5011304. URL <https://doi.org/10.1021%2Fnn5011304>.

B L Taylor and D E Koshland. Intrinsic and extrinsic light responses of *Salmonella typhimurium* and *Escherichia coli*. *Journal of Bacteriology*, 123(2):557–569, aug 1975. 10.1128/jb.123.2.557-569.1975. URL <https://doi.org/10.1128%2Fjb.123.2.557-569.1975>.

Barry L. Taylor, Igor B. Zhulin, and Mark S. Johnson. Aerotaxis and Other Energy-Sensing Behavior in Bacteria. *Annual Review of Microbiology*, 53(1):103–128, oct 1999. 10.1146/annurev.micro.53.1.103. URL <https://doi.org/10.1146%2Fannurev.micro.53.1.103>.

BJ Toley and NS Forbes. Motility is critical for effective distribution and accumulation of bacteria in tumor tissue. *Integr Biol (Camb)*, 4:165–76, Feb 2012.

J. F. Toso. Phase I Study of the Intravenous Administration of Attenuated *Salmonella typhimurium* to Patients With Metastatic Melanoma. *Journal of Clinical Oncology*, 20(1):142–152, jan 2002. 10.1200/jco.20.1.142. URL <https://doi.org/10.1200%2Fjco.20.1.142>.

Mahama A. Traore, Carmen M. Damico, and Bahareh Behkam. Biomanufacturing and self-propulsion dynamics of nanoscale bacteria-enabled autonomous delivery systems. *Applied Physics Letters*, 105(17):173702, oct 2014. 10.1063/1.4900641. URL <https://doi.org/10.1063%2F1.4900641>.

Mark C. M. van Loosdrecht, Willem Norde, Johannes Lyklema, and Alexander J. B. Zehnder. Hydrophobic and electrostatic parameters in bacterial adhesion. *Aquatic Sciences*, 52(1):103–114, mar 1990. 10.1007/bf00878244. URL <https://doi.org/10.1007%2Fbf00878244>.

Carlos H. Villa, Aaron C. Anselmo, Samir Mitragotri, and Vladimir Muzykantov. Red blood cells: Super-carriers for drugs biologicals, and nanoparticles and inspiration for advanced delivery systems. *Advanced Drug Delivery Reviews*, 106:88–103, nov 2016. 10.1016/j.addr.2016.02.007. URL <https://doi.org/10.1016%2Fj.addr.2016.02.007>.

Songzhi Xie, Long Zhao, Xiaojie Song, Maosheng Tang, Chuanfei Mo, and Xiaohong Li. Doxorubicin-conjugated *Escherichia coli* Nissle 1917 swimmers to achieve tumor targeting and responsive drug release. *Journal of Controlled Release*, 268:390–399, dec 2017. 10.1016/j.jconrel.2017.10.041. URL <https://doi.org/10.1016%2Fj.jconrel.2017.10.041>.

Xiao Xu, Yang Chen, Hejia Wei, Bin Xia, Feng Liu, and Na Li. Counting Bacteria Using Functionalized Gold Nanoparticles as the Light-Scattering Reporter. *Analytical Chemistry*, 84(22):9721–9728, oct 2012. 10.1021/ac302471c. URL <https://doi.org/10.1021%2Fac302471c>.

M Zhao, M Yang, XM Li, P Jiang, E Baranov, S Li, M Xu, S Penman, and RM Hoffman. Tumor-targeting bacterial therapy with amino acid auxotrophs of GFP-expressing *Salmonella typhimurium*. *Proc Natl Acad Sci U S A*, 102:755–60, Jan 2005.

S Zhou, C Gravekamp, D Bermudes, and K Liu. Tumour-targeting bacteria engineered to fight cancer. *Nat Rev Cancer*, 18:727–743, Dec 2018.